NONDESTRUCTIVE MATERIAL EVALUATION OF GRAY CAST IRON USING DC BIAS ALTERNATING MAGNETIC FIELD

S. Mio, K. Kawada and N. Kanemaru
Graduate School of Engineering, Oita University, Oita 870-1192, Japan

Y. Gotoh
Faculty of Science and Technology, Oita University, Oita 870-1192, Japan

Abstract

The gray cast iron is used in many machine parts such as pulleys, since it has excellent vibration damping, wear resistance, and castability. Material evaluation of this cast iron is important for quality assurance of machine products. This research proposes a method to identify defective products mixed with good products. Currently, test methods such as Brinell hardness and tensile strength tests are commonly used to check the quality of cast irons. However, these methods are not suitable for inspecting all products in terms of time required. Therefore, it is important to establish an electromagnetic nondestructive test that enables non-contact and fast measurement. It has been found that the use of AC magnetic fields in nondestructive testing methods can be used to measure defective gray cast iron. In this paper, we propose an electromagnetic non-destructive testing method that uses a DC-biased sinusoidal magnetic field, which enables measurements with higher sensitivity than those obtained with AC magnetic fields. The effectiveness of the proposed method is demonstrated through electromagnetic field finite element method (FEM) analysis using the play model method and corroborated by verification experiments.

Keywords: *electrical conductivity, gray cast iron, hysteresis magnetization curve, play model method*

Introduction

Generally, when making castings, defective products occur due to various factors such as machinery, materials, environment, and management systems. This research proposes a method to identify defective products that have been mixed into EN-GJL-250. The pulleys used in this research were for agricultural machinery and had a strength equivalent to EN-GJL-100, which was damaged during operation. Such an accident during an operation is expected to lead to a serious accident. It is therefore important to check the quality of gray cast iron.[1–3] The mechanical properties of gray cast iron are influenced by the microstructure, such as the ferrite/pearlite ratio. The defective products used in this research were found to have a high ferrite content and a low pearlite content. The electromagnetic properties of pearlite and ferrite are different. In general, ferrite has a higher electromagnetic permeability than pearlite. Therefore, the hysteresis magnetization properties and electrical conductivity of gray cast iron also depend on their content. Research to date has shown that electromagnetism can be used to deal with defective products due to microstructural changes.[4,5] Therefore, flawed gray cast iron can be evaluated nondestructively using electromagnetic sensors. Electromagnetic nondestructive testing is a useful method for quality assurance because it allows all products to be measured at high speed and low cost. Previous research has shown that it is possible to identify defective gray cast iron using alternating current.[4] This paper proposes a more sensitive electromagnetic non-destructive testing method for the evaluation of defective gray cast iron. In this method, an alternating magnetic field with a DC-biased sine wave is applied to gray cast iron, and the defects of the gray cast iron are evaluated from changes in the minor loop magnetic properties inside the cast iron. The

usefulness of the proposed method was examined by analyzing the alternating electromagnetic field using a 3D FEM that takes into account the minor loop magnetic properties of gray cast iron and by conducting verification experiments.

Microstructure Ratio and Electromagnetic Properties of Gray Cast Iron

Microstructure Ratio of Gray Cast Iron

In this research, EN-GJL-250 gray cast iron was evaluated as a good product, while gray cast iron with strength

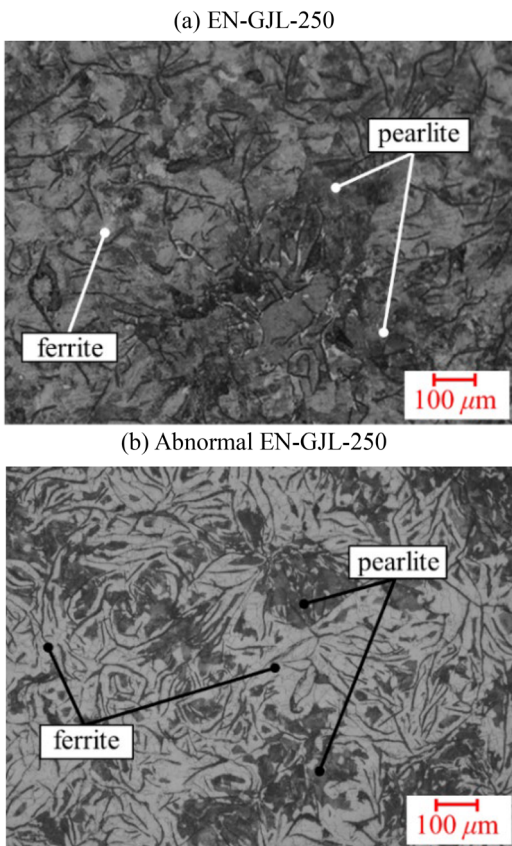**Figure 1. Damaged pulley and cut-out specimen (a) EN-GJL-250 (b) Abnormal EN-GJL-250.**

(a) EN-GJL-250

(b) Abnormal EN-GJL-250

Figure 2. Micrograph of (a) EN-GJL-250, (b) Abnormal EN-GJL-250.

Table 1. Chemical Composition of Gray Cast Iron

	C	Si	Mn	P	S	Cu	CE
EN-GJL-250	3.51	2.45	0.78	0.032	0.068	0.54	4.33
Abnormal EN-GJL-250	3.60	2.55	0.67	0.030	0.048	0.49	4.45

Table 2. Metallographic Ratios (Ferrite, Pearlite, and Graphite Area Fraction) and Brinell Hardness of Cast Irons

Metallographic structure	EN-GJL-250	Abnormal EN-GJL-250
Ferrite	0.7 %	61.0 %
Pearlite	99.3 %	39.0 %
Graphite area ratio	11.7 %	19.8 %
Brinell hardness	190 HBW	96 HBW

equivalent to EN-GJL-100 that broke during operation was evaluated as a defective product. Figure 1 shows the actual pulleys that failed and the shape of the test specimens. The pulley shown in Figure 1 does not show a localized reduction in strength, but rather a reduction in the strength of the entire product. Figure 2 shows the metallographic distribution ratio of gray cast iron. Figure 2a shows EN-GJL-250, and Figure 2b shows abnormal EN-GJL-250. Figure 2a shows that good gray cast iron has low ferrite content and high pearlite content. On the other hand, Figure 2b shows that the defective product has high ferrite content and low pearlite content. Table 1 shows the chemical composition. Table 2 also shows the metallographic ratios (ferrite, pearlite, and graphite area fraction) and Brinell hardness of the two parts.

Electromagnetic Properties of Gray Cast Iron

Figure 3 shows the hysteresis magnetization curves for EN-GJL-250 and abnormal EN-GJL-250. This figure denotes that the maximum electromagnetic permeability of abnormal EN-GJL-250 is larger than that of EN-GJL-250. On the other hand, the coercive force and residual flux density of abnormal EN-GJL-250 are lower than EN-GJL-250 cast iron. The electrical conductivity of EN-GJL-250 and abnormal EN-GJL-250 is shown in Figure 4. The electrical conductivity of abnormal EN-GJL-250 is 8.89 % lower than that of EN-GJL-250. These changes in electromagnetic properties may be influenced by the ferrite/pearlite ratio and graphite area fraction. An increase in ferrite increases the electromagnetic permeability of cast iron, while an increase in graphite area ratio decreases the
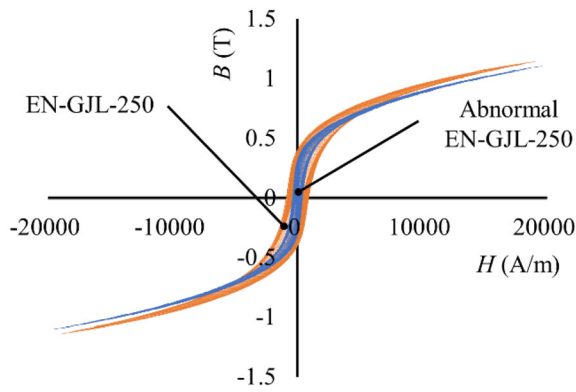
Figure 3. Hysteresis magnetization curves of EN-GJL-250 and abnormal EN-GJL-250 (0.1 Hz, 100 loops).
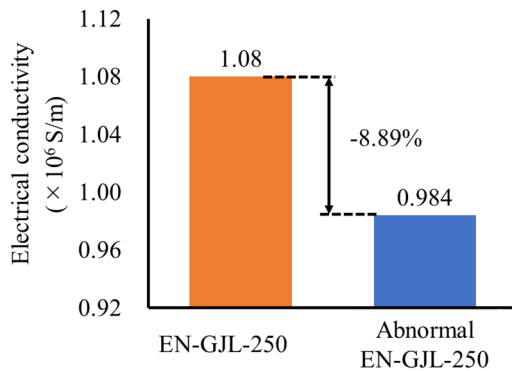

Figure 4. Electrical conductivity of EN-GJL-250 and EN-GJL-250 cast iron.

electrical conductivity. Therefore, this research proposes an electromagnetic nondestructive inspection method to identify defective cast irons based on the changes in the electromagnetic properties of cast irons.

Inspection Model and Application Conditions

Figure 5 shows an electromagnetic sensor for measuring the material evaluation of a gray cast iron pulley. Figure 5a shows a bird's-eye view of the inspection model, and Figure 5b shows a cross-sectional view in the x-z plane. Figure 6 also shows the excitation current waveforms used in this research.

The sensor consists of an excitation coil (80 turns, 0.5 φ) wound around the top of a U-shaped yoke laminated with silicon steel plates and a detection coil (40 turns, 0.2 φ) wound around one leg. The distance (Lift-off: L_o) between the gray cast iron and the proposed electromagnetic sensor is 0.1 mm. A DC-biased sine wave is applied to the excitation coil, and the magnetic flux density B_z in the z-direction inside the magnetic yoke material is detected by the detection coil. In previous research, the appropriate conditions for material evaluation of gray cast iron using only AC are a frequency of 500 Hz and an AC of 0.2 A.[4] Therefore, using
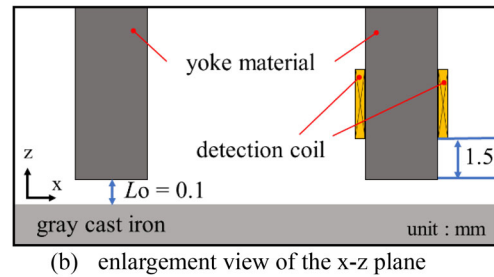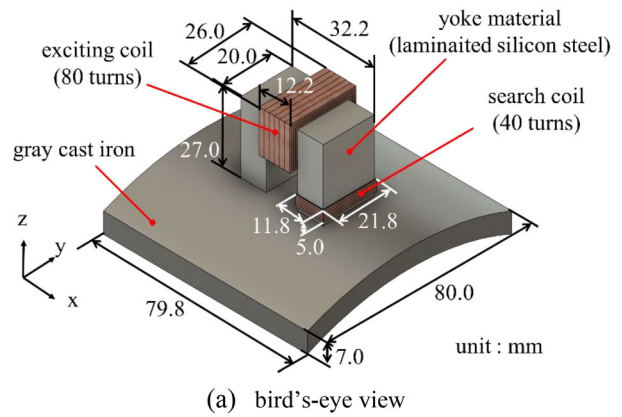

(a) bird's-eye view

(b) enlargement view of the x-z plane

Figure 5. Electromagnetic inspection model for detecting defective gray cast iron.
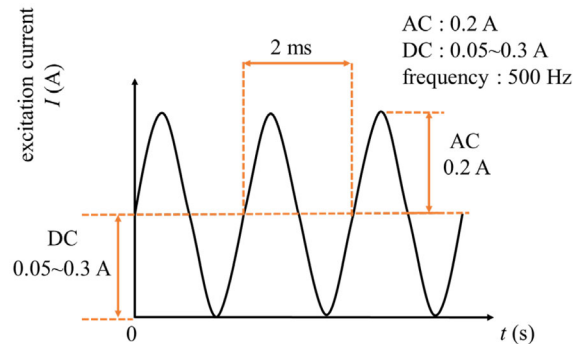

Figure 6. Excitation current waveform.

these excitation conditions as a reference, the optimum distribution of AC and DC components is verified by changing the DC component step by step. In addition, an evaluation comparison will also be made between the case where the applied magnetic field is only a sinusoidal AC magnetic field and the case where the applied magnetic field is a DC bias AC magnetic field. The AC current is kept fixed at 0.2 A, while the DC bias current was varied from 0.05 A to 0.3 A for the DC component only.

Appropriate Excitation Conditions

Figure 7 shows the rate of change of the magnetic flux density B_z inside the detection coil of the proposed sensor
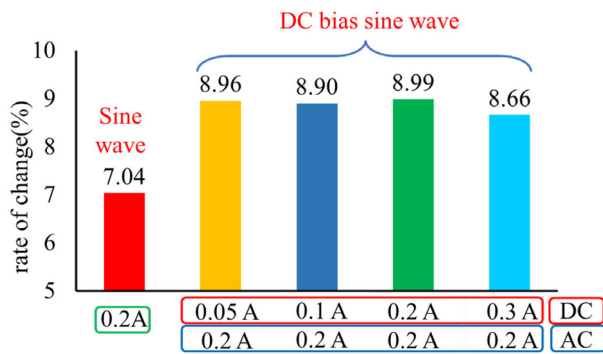
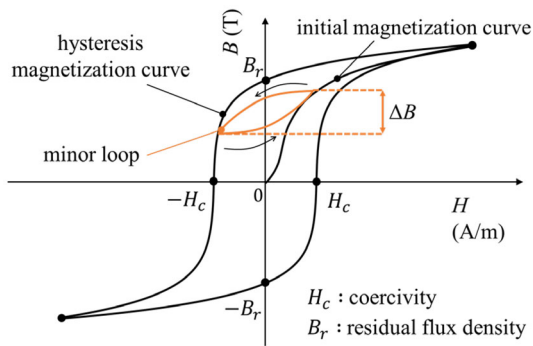**Figure 7. Rate of change in magnetic flux density of EN-GJL-250 and abnormal EN-GJL-250 (500Hz constant).**

Figure 8. Magnetic flux density changes in minor loops and cast iron.

Figure 9. Calculation area for magnetic flux density changes (x = 1.04mm, y = 0.05mm, z = 0.2mm).

Table 3. Calculated Results of Flux Density (B_{xp-p}) in Cast Iron for EN-GJL-250 and Abnormal EN-GJL-250 Under Each Applied Magnetic Field (500Hz constant)

Excitation current waveform	AC magnetic field only	DC bias AC magnetic field
EN-GJL-250 (B_{xp-p})	1.75×10^{-2} T	3.00×10^{-2} T
Abnormal EN-GJL-250(B_{xp-p})	1.58×10^{-2} T	2.14×10^{-2} T
Rate of change	11.4 %	39.9 %

Figure 9 shows the calculation area of magnetic flux density changes inside cast iron. The peak-to-peak value of the magnetic flux density change in the *x*-direction within this region is calculated. Table 3 shows the calculated results of changes in the magnetic flux density (B_{xp-p}) in the *x*-direction inside the cast iron. These results are for both normal and abnormal conditions of the cast iron under each applied magnetic field. The excitation current is 0.2A when only an AC magnetic field is applied. In the case of a DC-biased AC magnetic field, both the DC and AC currents are set at 0.2A. The frequency is constant at 500 Hz. This table denotes that the B_{xp-p} is greater with a DC bias AC magnetic field than with an AC magnetic field alone. Therefore, applying a DC-biased AC magnetic field is more suitable for material evaluation of gray cast iron than applying only an AC magnetic field.

Experimental and Analytical Results

Experimental Results

Figure 10 shows the measured magnetic flux density obtained within the detection coil when EN-GJL-250 and abnormal EN-GJL-250 are measured using the proposed sensor. The DC bias AC magnetic field waveform is a combination of both DC and AC sine waves, each set at

for EN-GJL-250 and abnormal EN-GJL-250 at each excitation current. This figure illustrates that the rate of change is greater when a DC-biased AC magnetic field is applied than when only an AC magnetic field is applied. Moreover, when a DC-biased AC magnetic field is applied, the rate of change is greatest when the DC and AC currents are both 0.2A. Then, a 3D nonlinear electromagnetic field FEM is used to understand this phenomenon. When a DC bias AC magnetic field is impressed on the ferromagnetic material such as cast iron, the magnetic properties inside the cast iron become minor loop magnetic properties. Therefore, it is necessary to consider the minor loop magnetic properties and eddy currents in cast iron for the electromagnetic field analysis. The minor loop magnetization curves are material-specific magnetic properties that occur inside the hysteresis magnetization curve, as shown in Figure 8. In this analysis, the flux density variation inside the cast iron is calculated by electromagnetic field analysis using a play model method that takes into account minor loop magnetization curves and eddy currents inside the cast iron.
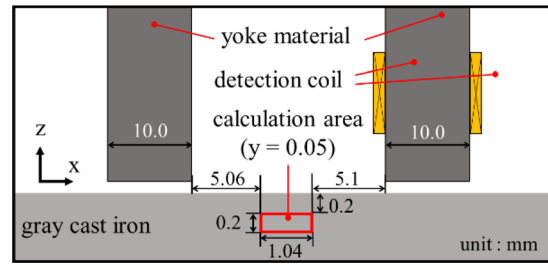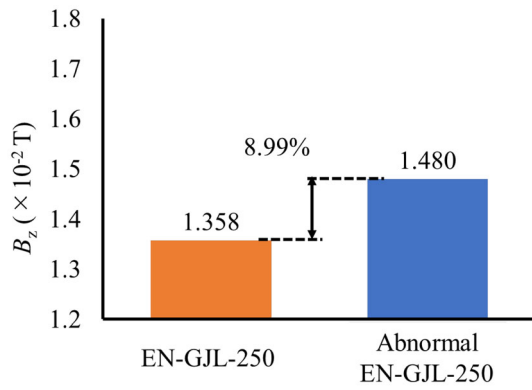
Figure 10. Flux density B$_z$ in the search coil of the proposed sensor (measured, DC: 0.2A, AC: 0.2A, 500 Hz constant).

0.2A, respectively. The excitation frequency is 500Hz. This figure denotes that the flux density B_z in the detection coil is increased when the abnormal EN-GJL-250 is measured. From this result, the electromagnetic sensor proposed can detect abnormal EN-GJL-250.

Analytical Results

Figure 11 shows the calculated magnetic flux density B_z obtained within the detection coil when EN-GJL-250 and abnormal EN-GJL-250 are measured using the proposed sensor. This figure shows that the magnetic flux density $\boldsymbol{B}_z$ is higher in abnormal EN-GJL-250 than in EN-GJL-250. Although the value of magnetic flux density B_z obtained in these calculations differs from the experimental results, it still exhibits the same tendency to increase in abnormal EN-GJL-250. Therefore, the electromagnetic sensor proposed can detect abnormal EN-GJL-250.
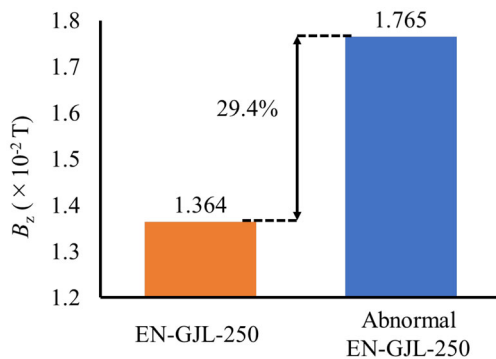

Figure 11. Flux density B$_z$ in the search coil of the proposed sensor (calculated, DC: 0.2A, AC: 0.2A, 500 Hz constant).

Discussion

Methods for Modeling Hysteresis Magnetization Curves

As this inspection method uses DC-biased sinusoidal waves, it is necessary to consider the residual flux density and coercive force inside the cast iron. Therefore, the 'Play model method'[6–10] is applied in this electromagnetic field analysis as a method to consider the hysteresis magnetization curve and electrical conductivity of EN-GJL-250 and abnormal EN-GJL-250. The play model method can represent the hysteresis characteristics using the play hysteron shown in Figure 12. Hs in the figure indicates the saturation magnetic field. The play hysteron is represented by equation (1), and the condition for the saturation magnetic field is given by Eqn. 2. In Eqn. 1, p_0 represents the value of p in the previous steps, and ζ represents the intercept on each axis in Figure 12. In the play model method, the hysteresis loop is created by dividing the value from the origin to the saturation field Hs into equal parts and stacking an equal number of play hysterons. The intercept ζ of each play hysteron can be calculated from Eqn. 3.

$$p(H, \zeta) = \max(\min(p_0, \ H + \zeta), \ H - \zeta) \qquad \text{Eqn. 1}$$

$$p = \begin{cases} H_s - \zeta (H > H_s) \\ -H_s + \zeta \ (H < -H_s) \end{cases} \qquad \text{Eqn. 2}$$

$$\zeta_n = (n - 1) \times (H_s/N_p) \ (1 \leqq n \leqq N_p) \qquad \text{Eqn. 3}$$

In Eqn. 3, ζ_n is the intercept in each loop and N_p is the number of divisions. The hysteresis curve can be expressed more accurately as the number of divisions N_p increases. The play hysteron p_n expressed from Eqns. 1 and 3 is given, where p_n^0 is the p_n value of the previous step and ζ_n is the value of the hysteron intercept at each step. However, the saturation field H_s cannot affect the magnetic flux density $\boldsymbol{B}$; therefore, p must be converted to $\boldsymbol{B}$. The flux density $\boldsymbol{B}$ can be calculated by multiplying the play hysteron p_n by the shape function f_n. The play hysteron p_n is multiplied with the shape function f_n for each division within each play hysteron. And the total play hysteron p_n
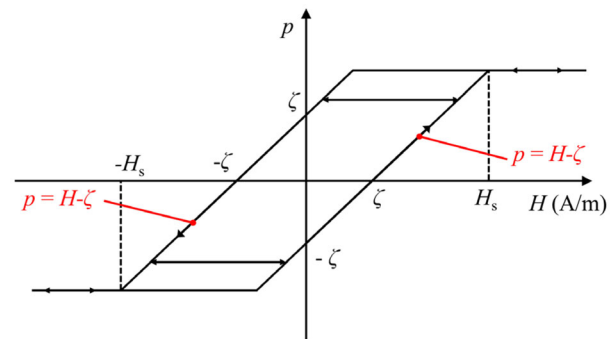

Figure 12. Play hysteron considering the saturated magnetic field.

obtained by adding them is expressed as the flux density B in Eqn. 4.

$$p_n(H, \zeta_n) = \max\big(\min(p_n^0, H + \zeta_n), H - \zeta_n\big) \quad (1 \leqq n \leqq N_p)\# \qquad \text{Eqn. 4}$$

$$B(H) = \sum_{n=1}^{N_p} f_n(p_n(H)) \;\; (1 \leqq n \leqq N_p) \qquad \text{Eqn. 5}$$

Nonlinear electromagnetic field analysis conditions

In this research, the A-ϕ method is used as the calculation method for eddy currents and alternating magnetic fields. The basic equations for electromagnetic field analysis considering eddy currents by the A-ϕ method are Eqns. 6 and 7, where A is the magnetic vector potential, ϕ is the electric scalar potential, σ is the electrical conductivity, v is the magneto-resistivity, and J_0 is the current density.
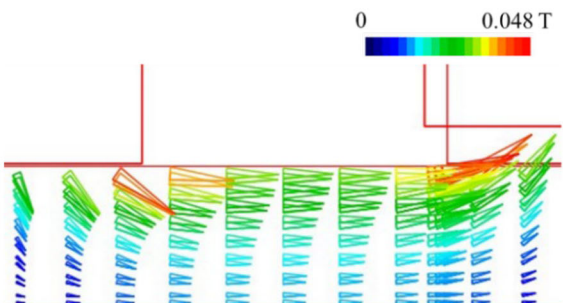
$$rot(v\text{rot } A) = J_0 - \sigma\big(\tfrac{\partial A}{\partial t} + \text{grad } \phi\big) \qquad \text{Eqn. 6}$$
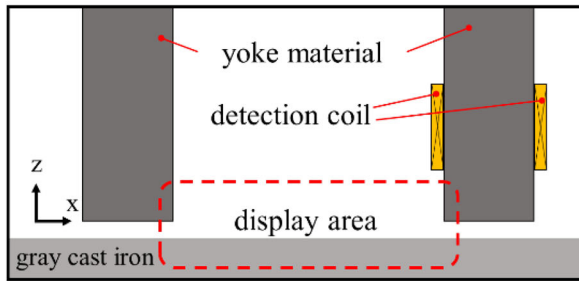
(a) Display area of flux density distribution
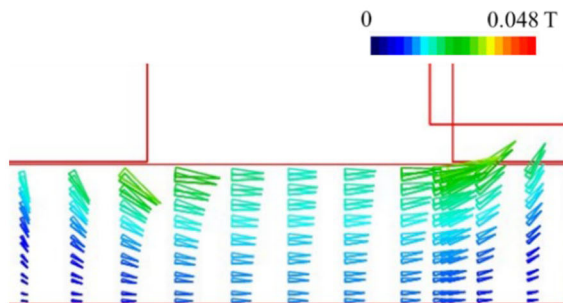
(b) EN-GJL-250 ($B_{\max}$ = 0.034 T)

(c) Abnormal EN-GJL-250 ($B_{\max}$ = 0.048 T)

Figure 13. Distribution of magnetic flux density inside the EN-GJL-250 and abnormal EN-GJL-250 (DC:0.2A, AC: 0.2A, 500 Hz constant).

$$div\big\{-\sigma\big(\tfrac{\partial A}{\partial t} + \text{grad } \phi\big)\big\} = 0 \qquad \text{Eqn. 7}$$

Magnetic flux density distribution inside the gray cast iron

The distribution of the flux density inside EN-GJL-250 and abnormal EN-GJL-250 is evaluated by electromagnetic field FEMof each play hysteron ca analysis using a play model method using hysteresis magnetization curves and eddy currents. Figure 13 shows the distribution of the flux density in the surface layer of the EN-GJL-250 and abnormal EN-GJL-250. Figure 13a shows the display area within these gray cast irons. Figure 13b and c shows the flux density distribution in EN-GJL-250 and abnormal EN-GJL-250, respectively. The excitation current waveform is the DC-biased sine wave shown in Figure 6. The frequency is 500 Hz, and both the DC and AC currents are set at 0.2A. These figures denote that the magnetic flux density inside the abnormal EN-GJL-250 is larger than that of the EN-GJL-250. This may be due to the effect of differences in the cast iron's electromagnetic permeability and electrical conductivity.

The electromagnetic permeability increases as the ferrite content increases. Therefore, the magnetic field entering the cast iron increased and the output signal increased. Also, as the electrical conductivity decreased, the eddy current generation decreased and the antiferromagnetic field weakened, resulting in an increase in the output signal. Taken together, the experimental and analytical results of this study suggest that the anomalous EN-GJL-250 exhibits a larger output signal than EN-GJL-250.

Conclusions

This research aimed to develop a more sensitive non-contact method for measuring the material evaluation of gray cast iron, which constitutes the pulleys used in power transmission, using electromagnetic sensors. For this purpose, comparative verification was carried out using two different excitation waveforms and several different current values. A three-dimensional finite element method using the play model method was also used to understand the phenomena. The results are summarized below.

1. There is a difference in the ratio of ferrite to pearlite between EN-GJL-250 and abnormal EN-GJL-250. The abnormal EN-GJL-250 with high ferrite content has lower Brinell hardness and higher maximum electromagnetic permeability. The coercive force and residual flux density in the hysteresis curve are also lower than the EN-GJL-250. The electrical conductivity of abnormal EN-GJL-250 is about 8.89% lower than that of EN-GJL-250.

2. By the use of an electromagnetic sensor, we were able to evaluate the material of gray cast iron. It was also found that the use of a DC-biased AC magnetic field enabled measurement with higher sensitivity than the application of an AC magnetic field alone. It was also found that the optimum distribution of current values in the DC-biased AC magnetic field was 0.2 A for both the DC and AC components.

REFERENCES

1. S.H. Khan, F. Ali, A.N. Khan, M.A. Iqbal, Pearlite determination in plain carbon steel by eddy current method. J. Mater. Process. Technol. **200**, 316–318 (2008). https://doi.org/10.1016/j.jmatprotec.2007.09.003
2. G. Vértesy, I. Tomáš, B. Skrbek, T. Uchimoto, T. Takagi, Investigation of cast iron matrix constituents by magnetic adaptive testing. IEEE Trans. Magn. **55**(3), 1–6 (2019). https://doi.org/10.1109/TMAG.2019.2892683
3. N.G. Prabhu Gaunkar, I.C. Nlebedim, G.V. Prabhu Gaunkar, D.C. Jiles, Examining the correlation between microstructure and barkhausen noise activity for ferromagnetic materials. IEEE Trans. Magn. (2015). https://doi.org/10.1109/TMAG.2015.2447833
4. S. Mio, K. Kawada, Y. Okumura, Y. Gotoh, Estimation of anomalous portion in gray cast iron using non-contacting electromagnetic sensor. IEEE Trans. Magn. (2023). https://doi.org/10.1109/TMAG.2023.3279844
5. K. Kawada, M. Kuromizu, Y. Gotoh, Simultaneous estimation cementite content and non-contact distance in spheroidal graphite cast iron using electromagnetic sensor. Int. J. Appl. Electromagn. Mech. **1**, S437–S447 (2023). https://doi.org/10.3233/JAE-220201
6. T. Matsuo, Anisotropic vector hysteresis model using an isotropic vector play model. IEEE Trans. Magn. **46**, 3041–3044 (2010). https://doi.org/10.1109/TMAG.2010.2043822
7. D. Lin, P. Zhou, A. Bergqvist, Improved vector play model and parameter identification for magnetic hysteresis materials. IEEE Trans. Magn. **50**, 357–360 (2014). https://doi.org/10.1109/TMAG.2013.2281567
8. M. Tohara, Y. Gotoh, Inspection method of outer side defect in ferromagnetic steel tube by insertion-type electromagnetic sensor using square wave alternating magnetic field with dc bias. IEEE Trans. Magn. (2021). https://doi.org/10.1109/TMAG.2020.3014337
9. S. Bobbio, G. Miano, C. Serpico, C. Visone, Models of magnetic hysteresis based on play and stop hysterons. IEEE Trans. Magn. **33**(6), 4417–4426 (1997). https://doi.org/10.1109/20.649875
10. T. Matsuo, M. Shimasaki, An identification method of play model with input-dependent shape function. IEEE Trans. Magn. **41**(10), 3112–3114 (2005). https://doi.org/10.1109/TMAG.2005.854892